draulic transition, its abruptness suggests a corresponding discontinuity in the sediment transport. One explanation, based on the assumption that transportability varies smoothly with grain size, is that the discontinuity in transport results from a gap in the size distribution of the sediment supply near the sand-gravel boundary (*27*, *28*). Figure 1 suggests an alternative explanation: A small increase in f_s [typically observed immediately upstream of the transition (*27*)] can produce a large increase in the relative transportability of sand and gravel. Where this occurs, τ^*_{ri} should decrease for both sand and gravel, but the decrease in τ^*_{rs} is proportionately larger (Fig. 1C). The resulting enhanced transportability of the sand will accelerate hydraulic sorting at the transition, such that sand, but not gravel, is able to proceed into the lower-energy environment downstream.

REFERENCES AND NOTES

1. J. H. Mackin, *Geol. Soc. Am. Bull.* **59**, 463 (1948); E. W. Lane, *Proc. Am. Soc. Civ. Eng.* **81**, 1 (1955).
2. M. T. Hill, W. S. Platts, R. L. Beschta, *Rivers* **2**, 198 (1991); F. K. Ligon, W. E. Dietrich, W. J. Trush, *Bioscience* **45**, 183 (1995); G. M. Kondolf and P. R. Wilcock, *Water Resour. Res.* **32**, 2589 (1996).
3. E. Meyer-Peter and R. Müller, *Proceedings of the 2nd Congress of the International Association for Hydraulic Research*, Stockholm (1948), p. 39; F. Engelund and E. Hansen, *A Monograph on Sediment Transport in Alluvial Streams* (Teknisk Vorlag, Copenhagen, 1972).
4. L. B. Leopold, in *Dynamics of Gravel-bed Rivers*, P. Billi, R. D. Hey, C. R. Thorne, P. Tacconi, Eds. (Wiley, Chichester, UK, 1992), chap. 14.
5. K. Ashida and M. Michiue, *Trans. Jpn. Soc. Civ. Eng.* **206**, 59 (1972).
6. G. Parker, P. C. Klingeman, D. L. McLean, *J. Hydraul. Div. Am. Soc. Civ. Eng.* **108**, 544 (1982).
7. Much of the size variation in sand-gravel beds results from spatial variation in sand content, which can be consistently correlated with sand proportion on the bed surface, visually estimated, mapped at the reach scale, and spatially averaged. Size variation within the sand and gravel fractions requires local samples [P. R. Wilcock *et al.*, *Water Resour. Res.* **32**, 2897 (1996)].
8. Size distributions used throughout this report are those of the bulk bed.
9. H. Ikeda and F. Iseya, *Env. Res. Center Paper No. 12,* University of Tsukuba, Japan (1988).
10. R. Bagnold, *Proc. R. Soc. London Ser. A* **372**, 453 (1980).
11. R. A. Kuhnle, in (*4*), chap. 7.
12. Dimensionless critical shear stress is $\tau^*_{ci} = \tau_{ci}/[(\rho_s - \rho)gD_i]$, where ρ_s and ρ are sediment and fluid density, g is gravity, D_i is grain size, and the subscript i is either s for sand or g for gravel. τ^*_c approximates the ratio of the drag force acting on a grain to its weight. Standard values of τ^*_c are summarized in M. C. Miller, I. N. McCave, P. D. Komar, *Sedimentology* **24**, 507 (1977) and recently reviewed by J. M. Buffington and D. R. Montgomery, *Water Resour. Res.* **33**, 1993 (1997).
13. J. D. Fenton and J. E. Abbott, *Proc. R. Soc. London Ser. A* **352**, 523 (1977).
14. E. D. Andrews, *Geol. Soc. Am. Bull.* **94**, 1225 (1983).
15. P. A. Carling and N. A. Reader, *Earth Surf. Processes Landforms* **7**, 349 (1982).
16. In a series of experimental runs in a small flume (*9*), water discharge, water depth, and sediment feed rate were held constant and the percentage of sand S in the sediment feed was varied from run to run. For $S \leq 20$, the observed transport followed the relation for pure gravel. For $S \geq 50$, the transport matched that of a pure sand feed. For $S = 30$ and 40, the observed transport was intermediate between that of sand and gravel. Although a clear transition between sand and gravel behavior was demonstrated, the small flow depths, large Froude numbers, and narrow bimodal size distribution used prevented direct extrapolation to the field case.
17. W. L. Jackson and R. L. Beschta, *Earth Surf. Processes Landforms* **7**, 517 (1982); P. A. Carling, *ibid.* **8**, 1 (1983); P. Diplas and G. Parker, *Proj. Rep. 190*, St. Anthony Falls Lab, University of Minnesota (1985); F. Iseya and H. Ikeda, *Geogr. Ann.* **69A**, 15 (1987); R. I. Ferguson, K. L. Prestegaard, P. J. Ashworth, *Water Resour. Res.* **25**, 635 (1989); R. Seal and C. Paola, *ibid.* **31**, 1409 (1995).
18. C. Paola and R. Seal, *Water Resour. Res.* **31**, 395 (1995).
19. W. W. Emmett, *U.S. Geol. Surv. Prof. Pap. 1139* (1980); _____, R. H. Myrick, H. A. Martinson, *U.S. Geol. Surv. Open-File Rep. 85-486* (1985); W. W. Emmett, R. H. Myrick, R. H. Meade, *U.S. Geol. Surv. Open-File Rep. 80-1189* (1980).
20. R. T. Milhous, thesis, Oregon State University, Corvallis (1973). See (*9*) for bed size distribution.
21. The size distributions used are those reported for bulk samples of the bed.
22. T. Lisle, *Water Resour. Res.* **25**, 1303 (1989).
23. P. R. Wilcock and B. W. McArdell, *ibid.* **29**, 1297 (1993).
24. P. R. Wilcock, in (*4*), chap. 6; *J. Hydraul. Eng.* **119**, 491 (1993); R. A. Kuhnle, *ibid.*, p. 1400.
25. Among various estimators for τ_{ci}, τ_{ri} is well scaled, reliably measured, and most directly related to the present goal of estimating transport rates [P. R. Wilcock, *Water Resour. Res.* **24**, 1127 (1988)]. Sand and gravel transport are scaled by their proportion in the bulk sediment bed, which is the only constant size distribution available for scaling transport rates and representing the influence of f_s on transport. The size distribution of the bed surface (on which transport immediately depends) is rarely known and varies with transport rate, so that a simple correlation between transport and bed grain size is not possible (*23*).
26. E. Yatsu, *Trans. Am. Geophys. Union* **36**, 655 (1955).
27. G. H. S. Smith and R. I. Ferguson, *J. Sediment. Res.* **A65**, 423 (1995).
28. G. Parker, in *Issues and Directions in Hydraulics*, T. Nakato and R. Ettema, Eds. (Balkema, Rotterdam, 1996), pp. 115–133.
29. I thank C. Paola, J. Pizzuto, and M. G. Wolman for comments on an earlier draft of this report. W. Emmett, R. Kuhnle, T. Lisle, and R. Milhous provided helpful discussion and supplementary information regarding their field data. Supported by U.S. Forest Service (Stream Systems Technology Center) Partnership Agreement 28-CCS5-019.

17 November 1997; accepted 25 February 1998

Formation of Carbonates in the Tatahouine Meteorite

J. A. Barrat, Ph. Gillet, C. Lécuyer, S. M. F. Sheppard, M. Lesourd

The Tatahouine meteorite, in southern Tunisia, shows terrestrial contamination that developed during 63 years of exposure on Earth's surface. Samples collected on the day of the fall in 1931 contained fractures, with no secondary minerals, whereas samples collected in 1994 contain calcite aggregates (70 to 150 micrometers) and rod-shaped forms (100 to 600 nanometers in length and 70 to 80 nanometers in diameter) on the fractures. Carbon isotope analysis of the carbonates within the Tatahouine meteorite [$\delta^{13}C = -2.0$ per mil Pee Dee belemnite standard (PDB)] and the underlying ground ($\delta^{13}C = -3.2$ per mil PDB) confirm their terrestrial origin.

The fall of the Tatahouine achondrite was observed on 27 June 1931 (*1*). The meteorite broke up along mineral grain boundaries at low altitude or upon impact. Hundreds of fragments were dispersed over a small strewnfield (<1 km^2) on a hill slope composed of Jurassic limestones with a desertic sandy soil. Many fragments were recovered that same day and sent to the Musée National d'Histoire Naturelle in Paris. The weights of the collected samples ranged from nearly 2 kg to 1 g or less. They were composed essentially of large orthopyroxene crystals (≤3 cm) with accessory chromite, iron sulfide, metal, and glass inclusions. The fragments were not highly brecciated by extraterrestrial shock events and display a partly recrystallized igneous texture. Tatahouine was classified as a diogenite (*1*), and this interpretation was confirmed by oxygen isotope systematics (*2*). The strewnfield was revisited in 1994 by Alain Carion, who recovered several small samples (<50 g) by sifting the first few centimeters of soil.

We examined samples and thin sections of Tatahouine collected in both 1931 and 1994. All the samples exhibit preexisting fractures, which were created either during the preterrestrial history of the meteorite or during its impact with Earth's surface. The fractures in the 1931

J. A. Barrat, Université d'Angers, Laboratoire de Géologie, 2 Boulevard Lavoisier, 49045 Angers Cedex, France.
Ph. Gillet, Institut Universitaire de France, and Laboratoire de Sciences de la Terre, Centre National de la Recherche Scientifique UMR 5570, Ecole Normale Supérieure de Lyon, 46 Allée d'Italie, 69364 Lyon Cedex 07, France.
C. Lécuyer and S. M. F. Sheppard, Laboratoire de Sciences de la Terre, Centre National de la Recherche Scientifique UMR 5570, Ecole Normale Supérieure de Lyon, 46 Allée d'Italie, 69364 Lyon Cedex 07, France.
M. Lesourd, Centre National de la Recherche Scientifique et Service Commun de Microscopie Electronique, Faculté de Medecine, Rue Haute de Reculée, 49045 Angers Cedex, France.

samples are empty and the surfaces are bright. Many of the fractures in the 1994 samples contain yellowish to light orange mineral aggregates. They occur as a partial filling with a rosette texture (Fig. 1A) or completely fill the fractures (about 100 μm wide) running throughout the centimeter-sized samples analyzed in this study. The rosettes are associated with saucer-shaped cavities (70 to 150 μm in diameter, 15 to 20 μm thick) in the orthopyroxene. The mineralogy of the aggregates is dominated by calcite (Fig. 2) as identified by micro-Raman spectroscopy (*3*). Carbonates rarely have been documented in meteorites, although they have been identified in some carbonaceous chondrites and martian meteorites (*4*). Calcite, dolomite, and breunnerite are usually observed but, in the case of the martian meteorite ALH84001, complex chemically zoned (Mg, Fe, Ca) carbonates occur.

Two arguments demonstrate without ambiguity the terrestrial origin of the carbonates. The mineralogical differences in the fractures between 1931 and 1994 indicate that the calcite fillings are no more than 63 years old. The carbon and oxygen isotope compositions of the carbonate (*5*) were measured on the fracture fillings, on one external surface coating (about 70 weight % $CaCO_3$), and in the sandy soil (about 6 weight % $CaCO_3$) immediately below the Tatahouine fragments. The fracture-filling carbonates and the coatings gave similar values ($\delta^{13}C = -2.0$ and -1.8 per mil PDB, $\delta^{18}O = +29.6$ and $+29.8$ per mil standard mean ocean water, respectively). The results obtained on the sandy soil are slightly lower ($\delta^{13}C = -3.2$ and $\delta^{18}O = +28.9$ per mil). Because the isotopic compositions of the fillings and the coating are similar to carbonate from the soil, we conclude that the fillings and the coatings result from solution and reprecipitation of the local sedimentary carbonates. The lack of a significant carbon isotope fractionation does not exclude formation of carbonates by biogenic processes.

We examined the Tatahouine achondrite under a field emission gun–scanning electron microscope (FEG-SEM) (*6*). At low magnification (Fig. 1A), the rosettes appear to be composed of a porous aggregate of small (≤10 μm) crystals of calcite, which was confirmed by Raman spectroscopy and qualitative energy dispersive spectroscopy (EDS) analyses, as well as traces of clay. No chemical zoning inside the rosettes was detected. At higher magnifications (×30,000 to ×230,000), the surfaces of some crystals display small rod-shaped forms with rounded ends 70 to 80 nm wide and ranging from 100 to 600 nm in length (Fig. 1, B to D); some of them look segmented (Fig. 1B). Small spheroidal forms (about 70 nm in diameter) are less frequent. In some places, the rod-shaped forms are so numerous that they appear to surround the crystals (Fig. 1D). Identical rod-shaped objects are found in the same open fractures, on the orthopyroxene (Fig. 1C) and chromite crystals, and on the external surfaces of the meteorite fragments (collected in 1994) that were in contact with the soil.

Similar rod-shaped objects have been described in the martian meteorite ALH84001 and have been proposed to be possible fossils of martian microbes (*7*). This interpretation is still vigorously disputed (*8, 9*), and four types of explanations for these forms are currently debated: (i) artifacts produced when the samples were being coated for observations under an electron microscope (*8, 10*); (ii) imaging artifacts related to the viewing angle under the electron beam (*8*); (iii) mineralogic (*8*); and (iv) very small bacteria or bacterial relicts (*7*). The artifact interpretation is not valid for our samples. Tatahouine chips, some with calcite aggregates and others just freshly broken and free of secondary minerals, were mounted together and then coated with carbon (*6*). No artifact was observed as a consequence of this coating process (Fig. 3). The rod-shaped forms are observed only on the carbonate-bearing fractures on carbonate, pyroxene, and rare chromite, and are thus unambiguously related to the terrestrial fluid-assisted alteration of the meteorite. Bradley *et al.* (*8*) have proposed in the case of ALH84001 that the rod-shaped forms could be high-temperature vapor-deposited magnetite whiskers or emergent substrate lamellae, which can mimic bacterial forms under certain viewing angles. This interpretation cannot be applied to Tatahouine for two reasons. (i) The carbonates formed at surface temperature (<60°C), and (ii) some of the rod-shaped forms are randomly clustered (Fig. 1D). When they

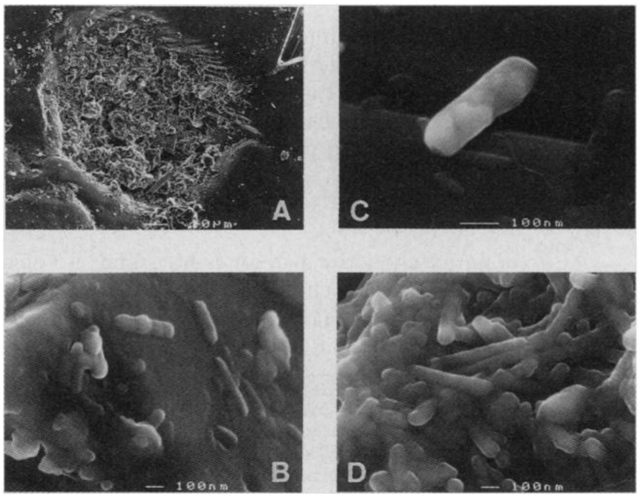

Fig. 1. (**A**) SEM image of a saucer-shaped calcite rosette on a fresh internal fracture surface of an orthopyroxene crystal [$(Mg, Fe)SiO_3$] from a sample collected in 1994 (bar = 10 μm). The porous aggregate rosette lies in a cusp in the pyroxene, suggesting a local dissolution feature of the silicate. The rosette is about 80 μm in diameter. (**B** to **D**) High-resolution FEG-SEM images showing rod-shaped and ovoid features. (B) The rod-shaped objects lie randomly on a crystallographic face of a single rhombohedral calcite crystal. (C) A rod-shaped object lies on an orthopyroxene surface near a carbonate rosette. Note the complex surface texture. (D) Typical cluster of rod-shaped and round-ended objects occasionally observed within the carbonate rosettes.

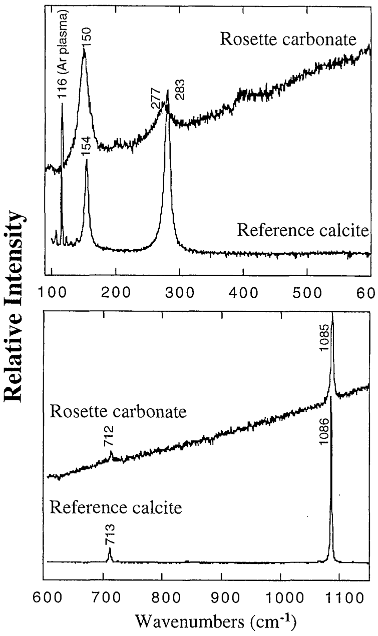

Fig. 2. Typical Raman spectrum recorded on a rosette compared with the spectrum of a pure calcite single crystal (*3*). A low laser power (10 mW) was used. At higher powers the sample, which was white, turned brown and then smoke was observed where the beam had been. The observed 4 to 5 cm^{-1} difference between the two spectra for the two low-lying frequency modes is consistent with about 100 K heating of calcite (*12*) under the spot. The noisy spectrum, absorption of the laser radiation, and strong fluorescence can be related to the presence of organic matter or to traces of transition elements like Fe^{3+} and Mn^{2+} (*13*).

occur as isolated individuals, no preferred orientation is observed with respect to crystallographic directions of the substrate carbonate (Fig. 1B) or pyroxene (Fig. 3B). Moreover, changing the viewing angle shows that they are not rooted in specific planes of the substrate minerals.

Further information on the rod-shaped forms can be inferred from EDS chemical analysis. The chemical composition of an individual rod cannot be determined directly because it is too small for EDS techniques. However, for the clusters with sizes of a few micrometers, a qualitative analysis is made possible. The inferred composition of the clusters is indistinguishable from that of the substrate calcite. The rods are thus either purely inorganic calcite-rich precipitates or mineralized organisms. Chemical analyses confirm that they cannot be magnetite or other iron oxides, iron hydroxides, or silicates. Similar forms 5 to 10 times larger are conventionally interpreted to be bacterial relicts (*11*). Although, there is no direct evidence for bacterial activity, we note that, in addition to the rod-shaped forms and their surface textures (Fig. 1D), there is an intimate association between the saucer-shaped depression in the pyroxene and the carbonates. The observed depressions could result from bacteria exploiting the immediate presence of chemical elements—carbon and calcium from the carbonates, and iron, silicon, and so forth from the orthopyroxenes.

We propose the following scenario for Tatahouine's residence on Earth. In 1931, the meteorite fell and was found with unfilled fractures. During the 63-year history of the meteorite in the desert soil, fluids transferred carbonates from the local sediments or soil to the meteorite, filling the preexisting fractures and locally coating the fragment surfaces. This demonstrates that meteorites can acquire terrestrial minerals in a very short time.

REFERENCES AND NOTES

1. A. Lacroix, *C. R. Acad. Sci. Paris* **193**, 305 (1931).
2. R. N. Clayton and T. K. Mayeda, *Geochim. Cosmochim. Acta* **60**, 1999 (1996).
3. The Raman data were collected with a DILOR XY micro-Raman spectrometer. A 100× objective was used to focus the beam of an argon laser (λ = 514.5 nm) to give a spot of 2 μm on the sample.
4. M. Zolensky and H. Y. McSween Jr., in *Meteorites and the Early Solar System*, J. F. Kerridge and M. S. Matthews, Eds. (Univ. of Arizona Press, Tucson, AZ, 1988), pp. 114–143; D. W. Mittlefehldt, *Meteoritics* **29**, 214 (1994); J. L. Gooding, S. J. Wentworth, M. E. Zolensky, *Geochim. Cosmochim. Acta* **52**, 909 (1988); B. Mason *et al.*, *Smithson. Contrib. Earth Sci.* **30**, 17 (1992); A. J. T. Jull, C. J. Eastoe, S. Cloudt, *J. Geophys. Res.* **102**, 1663 (1997).
5. Isotopic analyses were performed on CO_2 gas extracted by a H_3PO_4 acid technique with a VG-PRISM mass spectrometer. For the fracture-filling sample, three chips without coating (total weight 30 mg), with a few filled microfractures, were selected and leached with H_3PO_4 acid for 12 hours, yielding about 0.3 μmol of CO_2.
6. For the FEG-SEM observations and EDS chemical analyses, untreated samples with freshly exposed fractures were mounted on SPI carbon conductive adhesive tape followed by carbon coating with a Baltec modular high-vacuum coating system MED 020. The thickness of the carbon coating is difficult to estimate but is probably <15 nm. Operating conditions of the JEOL JSM6301-F microscope were 5 to 11 kV with a sample-to-objective working distance of 5 to 15 mm.
7. D. S. McKay *et al.*, *Science* **273**, 924 (1996).
8. J. P. Bradley *et al.*, *Nature* **390**, 454 (1997).
9. D. S. McKay *et al.*, *ibid.*, p. 455; R. A. Kerr, *Science* **278**, 1706 (1997).
10. R. L. Folk and F. L. Lynch, *J. Sediment. Res.* **67**, 583 (1997).
11. K. H. Nealson, *Annu. Rev. Earth Planet. Sci.* **25**, 403 (1997).
12. P. Gillet *et al.*, *Phys. Chem. Minerals* **20**, 1 (1993).
13. W. D. Bischoff *et al.*, *Am. Mineral.* **70**, 581 (1985); J. Urmos *et al.*, *ibid.* **76**, 641 (1991).
14. We are grateful to A. Carion and C. Perron (Musée National d'Histoire Naturelle) for generously donating the samples. We thank F. Albarède, P. Buseck, R. L. Folk, D. Rigomier, P. Thomas, P. Warren, and an anonymous reviewer for their constructive comments on the manuscript.

11 November 1997; accepted 20 February 1998

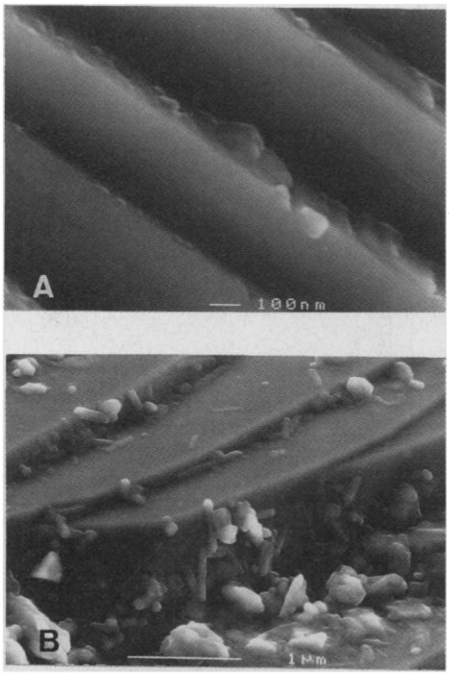

Fig. 3. Comparison of high-magnification FEG-SEM images of two pyroxene surfaces from the same Tatahouine sample. They were coated together on the same mount (6) to check for potential artifacts related to the coating procedures. (**A**) This surface was created by breaking the sample far away from any observed preexisting fractures. (**B**) This surface was near a rosette in a filled fracture. In both (A) and (B), the cleavages are observed. The rod-shaped forms are observed only in (B), ruling out a coating artifact for these features. Note also in (B) the random orientations of the rods.

Oxygen Isotopic Abundances in Calcium-Aluminum–Rich Inclusions from Ordinary Chondrites: Implications for Nebular Heterogeneity

Kevin D. McKeegan,* Laurie A. Leshin, Sara S. Russell,
Glenn J. MacPherson

The oxygen isotopic compositions of two calcium-aluminum–rich inclusions (CAIs) from the unequilibrated ordinary chondrite meteorites Quinyambie and Semarkona are enriched in ^{16}O by an amount similar to that in CAIs from carbonaceous chondrites. This may indicate that most CAIs formed in a restricted region of the solar nebula and were then unevenly distributed throughout the various chondrite accretion regions. The Semarkona CAI is isotopically homogeneous and contains highly ^{16}O-enriched melilite, supporting the hypothesis that all CAI minerals were originally ^{16}O-rich, but that in most carbonaceous chondrite inclusions some minerals exchanged oxygen isotopes with an external reservoir following crystallization.

CAIs in primitive chondrite meteorites are the oldest solid materials believed to have formed in the solar system (*1*, *2*). Studies of their mineralogy, chemical composition, and isotopic abundances have provided unique information regarding the thermal and chemical processing of materials during the earliest epoch of solar system formation (*3*). However, most previous studies examined CAIs from a relatively small group of meteorites (*4*), the carbonaceous chondrites (CCs), and most O isotopic measurements were restricted to only a few CCs that contain large and abundant CAIs. Thus, the extent to which inferences based on data from these CAIs can be generalized to the

---

K. D. McKeegan and L. A. Leshin, Department of Earth and Space Sciences, University of California Los Angeles, Los Angeles, CA 90095-1567, USA.
S. S. Russell and G. J. MacPherson, Department of Mineral Sciences, MRC NHB-119, National Museum of Natural History, Smithsonian Institution, Washington, DC 20560, USA.

*To whom correspondence should be addressed. E-mail: kdm@ess.ucla.edu